Available online at www.sciencedirect.com
ScienceDirect
Journal of Power Sources 162 (2006) 105–113
JOURNAL OF POWER SOURCES
www.elsevier.com/locate/jpowsour

Preliminary evaluation of an alkaline chitosan-based membrane fuel cell

Ying Wan, Brant Peppley *, Katherine A.M. Creber, V. Tam Bui, Ela Halliop

Department of Chemistry and Chemical Engineering, Royal Military College of Canada, P.O. Box 17000, Station Forces, Kingston, Ontario, Canada K7K 7B4

Received 2 June 2006; received in revised form 5 July 2006; accepted 6 July 2006
Available online 23 August 2006

Abstract

New polymer electrolyte composite membranes were prepared by using chitosan as the matrices and incorporating potassium hydroxide for ionic functionality. These membranes had a three-layer structure, which consisted of a porous intermediate layer and two crosslinked solid surface layers. Their ionic-conductive properties were investigated using impedance spectroscopy. Some composite membranes showed a conductivity near 10^{-2} S cm^{-1} after hydration for 1 h at room temperature. Several composite membranes were preliminarily integrated into fuel cells for the assessment of their electrochemical performance using hydrogen as fuel, air as oxidant and platinum as the electrode catalysts. A membrane electrode assembly was fabricated by directly pressing two gas-diffusion electrodes onto the two opposite surfaces of the composite membrane. All fuel cells showed an open-circuit potential around 1.0 V, and under appropriate running conditions, a current density of about 30 mA cm^{-2} was achieved. Some possible improvements on the performance of the resultant fuel cells are also suggested.

Keywords: Polymer electrolyte; Composite membrane; Chitosan; Alkaline fuel cell

1. Introduction

Polymer electrolyte membrane fuel cells have received attention for years because of their potential applications for portable power [1], and use in vehicles [2]. Up to now, these fuel cells are mainly run based on proton-conducting polymer membranes. Of the known proton-type membranes, the most widespread is a perfluorinated membrane, commercially known as Nafion [3], which is a kind of ionomer in which the ionic sites are grafted onto the skeleton of the polymer chain. Despite great successes with Nafion membranes, the cost of Nafion has limited the development of the corresponding fuel cells. In addition, it has also been found that the fuel cells, which employ Nafion membranes, are limited to the range of the temperature within which the membranes can be reliably used [4]. Moreover, when Nafion membranes are applied to direct methanol fuel cells (DMFCs), which is now increasingly believed to be the first fuel cell commercially likely to power portable devices [5], several major obstacles appear, such as a very wet environment and slow anode kinetics as well as parasitic methanol crossover [6–9]. Many efforts, therefore, are being directed towards developing new polymer electrolyte membranes [10]. Besides a great number of proton-type membranes, alkaline anion-exchange membranes have also aroused new interest since several potential advantages could be obtained if alkaline membranes were employed for DMFCs: (1) facile kinetics at both the cathode and anode [11]; (2) more effective oxidation of methanol in alkaline media [12,13]; (3) reduced level of methanol crossover from anode to cathode; (4) possibly cheaper non-noble metal catalysts (such as nickel and silver [14]); (5) more easily machined metal bipolar plates and minimal electrode weeping and component corrosion [15,16].

Besides pure polymer electrolyte membranes, ion-solvating polymer composite membranes are also quite commonly used in low-temperature (working temperature is lower than 100 °C) fuel cells. These composite membranes can be classified into acidic and alkaline membranes depending on whether the ionic functionality is protonic or hydroxylic. Alkaline ion-solvating polymer composite membranes are especially attractive because the fuel cells based on these types of membranes have potentially a much lower cost [17]. To date, several alkaline fuel cells using different ion-solvating polymer composite membranes have been developed [18–20]. One of relatively successful membranes is the poly(ethylene oxide)(PEO)-based membrane

* Corresponding author. Tel.: +1 613 541 6000x6702; fax: +1 613 542 9489.
E-mail address: peppley-b@rmc.ca (B. Peppley).

0378-7753/$ – see front matter © 2006 Elsevier B.V. All rights reserved.
doi:10.1016/j.jpowsour.2006.07.027

incorporated KOH, which shows a well-defined characteristic of voltage versus current density in alkaline fuel cells [21]. However, due to the high crystallinity of the PEO membrane, some drawbacks for this kind of membrane still remain [22,23].

Chitosan, a principal derivative of chitin, is a natural, low-cost biopolymer and also is a weak alkaline polymer electrolyte [24]. A chitosan membrane can retain its chemical and thermal stability up to 200 °C with an acceptable mechanical strength [25]. Furthermore, the presence of hydroxyl and amino groups on the backbone of chitosan also affords the chitosan membrane a higher level of hydrophilicity, which is crucial for the operation of polymer electrolyte membrane fuel cells [26]. Although chitosan is also a semi-crystalline polymer, the crystallinity of chitosan membranes can be greatly decreased using some crosslinking [27]. In its natural state (dry state), a chitosan membrane is almost non-conductive. However, when an appropriately crosslinked chitosan membrane is fully hydrated, it can have a conductivity close to 10^{-3} S cm^{-1} [28]. But this value is still not high enough for practical fuel cells. Therefore, from the characteristics of chitosan mentioned above, chitosan seems to be a suitable candidate to serve as a matrix for ion-solvating alkaline polymer composite membranes. Therefore, we have fabricated some alkaline chitosan-based composite membranes by incorporating KOH for ionic functionality [29] and have explored their use in alkaline fuel cells. In order to hold the KOH permanently inside the composite membrane, a special three-layer membrane structure was designed, which consisted of a porous intermediate layer and two crosslinked solid surface layers. In the present study, these composite membranes were integrated into fuel cells for a preliminary evaluation of their performance.

2. Experimental

2.1. Materials and reagents

Chitosan and the following chemicals were all obtained from Aldrich and used as received: acetic acid, sodium acetate, *N*-acetyl-D-glucosamine, potassium hydroxide pellets, glutaraldehyde (GA, 25% by weight in water), potassium hydroxide volumetric standard (0.1 M solution in water), hydrochloric acid volumetric standard (0.1 M solution in water). Gas-diffusion electrodes (1 mg cm^{-2} Pt dispersed into Vulcan XC-72 carbon black being 20 wt.% of the electrode) were purchased from ElectroChem Inc. (USA). The bipolar plates and cell fixtures were provided by DuPont Canada.

2.2. Degree of deacetylation and molecular weight of chitosan

The first derivative UV (ultraviolet) spectra of chitosan were collected using a CARY 5E UV–VIS–NIR spectrometer and they were utilized for calculating the degree of deacetylation (DDA) of chitosan [30]. A calibration curve from *N*-acetyl-D-glucosamine was generated according to Tan et al.'s method [31]. The viscosity-average molecular weight of chitosan was measured using 0.25 M CH_3COOH/0.25 M CH_3COONa as the solvent system with our previously reported method [32]. The DDA value and viscosity–average molecular weight of chitosan were determined as 72.5 (±2.2)% and 2.1 (±0.11) × 10^6, respectively.

2.3. Preparation of composite membrane

The preparation of composite membranes involved a two-step process. In the first step, powdered chitosan was dissolved in a 1.0% (by volume) aqueous acetic acid solution to produce a 1.0% (by weight) chitosan solution. To this solution, a known quantity of GA was added with vigorous stirring for 3 h at ambient temperature. The mixture was then cast into a membrane on a specially constructed Plexiglas dish designed for fitting into the fuel cell test assembly. The dish was placed in a chamber and the solvent was allowed to slowly evaporate while the membrane was slightly crosslinked at 25 °C for 48 h so that the membrane thus obtained was of a gelatinous nature at the end of this process. The dish was subsequently immersed into a pool containing a freshly prepared KOH aqueous solution with a known concentration for 24 h to incorporate potassium hydroxide into the membrane. The soft membrane in the dish was then dried in air for a given period of time, at which point the solid-like membrane was carefully peeled off the dish. The so produced membrane was placed in a hermetically sealed chamber to maintain its moisture content. This membrane became an intermediate layer in the further preparation of the composite membrane.

In the second step, a 1.0% (by weight) chitosan solution was prepared in the same way as in the first step, and allowed to be crosslinked in a flask at 25 °C for 48 h. This solution was then cast into a thin layer on a Plexiglas dish and then the membrane obtained in the first step was overlaid onto this liquid bottom layer. Finally, a top layer composed of the crosslinked chitosan solution was immediately cast onto the membrane. This three-layer composite membrane was then dried in air at 25 °C for around 4 days.

Two series of composite membranes were prepared by varying the amount of crosslinking agent or altering the concentration of KOH solution. One set was designated as CH/G-A, CH/G-B, CH/G-C, and CH/G-D; the other set was named as CH/K-4, CH/K-5, CH/K-6 and CH/K-7, respectively.

2.4. KOH content in the intermediate layer of composite membrane

The KOH load (ξ_{KOH}, wt.%) in the inner layer was determined using a gravimetric method and calculated via following relationship:

$$\xi_{KOH} = \frac{[(W_2 - W_1/D) \times C_0]}{W_0} \quad (1)$$

where W_1 is the total weight of the membrane and the dish before the dish was immersed in the KOH solution; W_2 the total weight of the membrane and the dish after the dish was taken out of the container and the KOH solution inside the dish was completely removed; C_0 (%, w/v) the concentration of the KOH solution; D the density of the KOH aqueous solution and it varies with C_0;

Table 1
Basic information of the composite membranes[a]

Membranes	GA/chitosan weight ratio in feed	C_0 (%)	ξ_{KOH} (wt.%)	Conductivity (S cm^{-1})[b,c]	
				Before hydration	After hydration
CH/G-A	0.0555:1	4	5.61(±0.11)	$1.26(\pm0.24)\times10^{-6}$	$1.25(\pm0.21)\times10^{-2}$
CH/G-B	0.0647:1	4	5.49(±0.12)	$1.19(\pm0.29)\times10^{-6}$	$1.21(\pm0.26)\times10^{-2}$
CH/G-C	0.0741:1	4	5.44(±0.13)	$1.24(\pm0.23)\times10^{-6}$	$1.17(\pm0.19)\times10^{-2}$
CH/G-D	0.0832:1	4	5.32(±0.11)	$1.28(\pm0.21)\times10^{-6}$	$1.24(\pm0.22)\times10^{-2}$
CH/K-4	0.0555:1	4	5.53(±0.12)	$1.09(\pm0.36)\times10^{-6}$	$1.19(\pm0.17)\times10^{-2}$
CH/K-5	0.0555:1	5	5.82(±0.15)	$1.13(\pm0.27)\times10^{-6}$	$1.62(\pm0.18)\times10^{-2}$
CH/K-6	0.0555:1	6	6.49(±0.13)	$1.74(\pm0.21)\times10^{-6}$	$2.26(\pm0.24)\times10^{-2}$
CH/K-7	0.0555:1	7	7.04(±0.11)	$2.69(\pm0.32)\times10^{-6}$	$3.14(\pm0.17)\times10^{-2}$

[a] The values listed in the table are average values from six specimens for each sample.
[b] Hydration time for conductivity measurements is 1 h.
[c] The thickness of the membrane in the dry state and in the swollen state is measured before and after hydration, respectively, and the corresponding average values are used for the calculation of the conductivity.

W_0 the dry weight of the chitosan. C_0 and calculated ξ_{KOH} for two sets of samples were listed in Table 1.

2.5. Degree of crosslinking of composite membrane

Since it was quite difficult to quantify the degree of crosslinking for these composite membranes because of some unwanted side reactions, an estimate of the degree of crosslinking for each composite membrane was made by using the GA/chitosan weight ratio in the feed as an approximation.

2.6. Ionic conductivity

The measurements of ionic conductivity were carried out using an AGILENT impedance analyzer (model 4294A) according to a published method [33]. Complex impedance spectra were recorded at ambient temperature by sandwiching dry membranes between a pair of brass-blocking electrodes in the measurement cell with an alternating current (a.c.) mode (frequency range: 0.1–10^4 kHz, amplitude of the a.c. signal: 0.5 V). For the measurements in the swollen state of the membranes, the membranes were immersed in water at room temperature for 1 h. Prior to any measurement, the surface water was gently removed, and then the swollen membrane was quickly placed between two electrodes in the measurement cell. Repeat measurements were performed and the ionic conductivity was averaged. In most cases, the bulk resistance of the composite membrane was directly obtained from the intercept of the complex impedance graph with the real axis. In some cases that impedance curves did not touch the real axis, the complex impedance plot was then extrapolated to its intersection with the real axis, and the conductivity of corresponding composite membrane was calculated with Osman's method [34].

2.7. Ion-exchange capacity (IEC) of composite membrane

A previously reported method [35,36] was used to determine the IEC. A piece of composite membrane with a given weight was immersed in a 0.1 M HCl standard solution (20 ml) at ambient temperature for 24 h with occasional stirring, and then the solution together with membrane was titrated back to neutralization with 0.1 M KOH standard solution. End-points were determined from the maximum points registered in the differential titration plots. Three repeats were conducted for each sample and a blank run (without membrane) was also performed. The IEC was calculated as follow:

$$\mathrm{IEC} = \frac{n_{\mathrm{HCl},i} - n_{\mathrm{HCl},f}}{m_{\mathrm{dry}}} \quad (2)$$

where $n_{HCl,i}$ is the HCl quantity (equivalent) in the initial solution (0.1 M, 20 mL), $n_{HCl,f}$, the remaining amount of HCl (equivalent) determined by the titration, and m_{dry} is the mass of the dry membrane sample.

2.8. Membrane electrode assembly (MEA)

Two surfaces of the composite membrane were slightly wetted using a very small amount of water. The composite membrane was allowed to stay in air for 5 min before it was used for MEA. Two electrodes of the same size were directly attached to the two opposite surfaces of the composite membrane and two stainless steel plates were respectively applied to each electrode. The MEA was made by pressing this assembly at 4 t for 10 min at 25 °C.

2.9. Determination of potential–current polarisation curves

The obtained MEA was incorporated into a single test fixture and the resultant unit cell was then installed into the Fuel Cell Automated Test Station (Hydrogenics Inc.). The cell was run under various operation conditions by changing the operation temperature and relative humidity as well as the flow rate of hydrogen and air (in most cases, the pressure ratio of hydrogen to air was kept at 103 kPa/103 kPa). The flow rate between hydrogen and air was always kept constant with a fixed ratio at 1 (H_2):4 (air) for all measurements. In order to examine the effect of the single operation condition, the cell was run while keeping all other operational conditions constant. The active surface area of the electrode was automatically recorded by the Test Station.

3. Results and discussion

3.1. Basic parameters of composite membrane

Under ideal reaction conditions, i.e., each GA molecule crosslinks two amino groups on two different chitosan chains and all other possible side reactions are negligible, an approximate calculation could be performed for the degree of crosslinking of chitosan membrane by considering the composition of initial reaction mixture, and the degree of crosslinking can be expressed as the fraction of bridges in the total number of network structural elements [37]:

$$\text{d.c.} = \frac{\chi}{\chi + (1 - 2\chi)} \times 100\% \quad (3)$$

where χ is the amount of crosslinking agent (in mole) introduced into the reaction per one mole of the aminosaccharide. However, in our case, ideal reactive results cannot be achieved because (1) some GA molecules may only react with one amino group (the other end of the GA molecule is free) or they do react with two amino groups but these two amino groups belong to the same chitosan chain; (2) those GA molecules which have not reacted with any amino group in the first step, will be simply dissolved into the KOH solution or water. Hence, it is nearly impossible to quantify the degree of crosslinking for these composite membranes. It may be feasible to use the GA/chitosan weight ratio in the feed as an approximate estimation for the degree of crosslinking of composite membrane assuming that the degree of crosslinking of composite membrane is closely related to or even proportional to the amount of GA used in the crosslinking reaction. In the following sections, the GA/chitosan weight ratio in the feed will be thus used as a substitution of the degree of crosslinking of the composite membrane. Although a relatively high KOH load may provide the resultant hydrated composite membranes with a higher conductivity, however, we found that composite membranes would show relatively poor mechanical properties if the KOH content was higher than ca. 12 wt.%. The KOH content, therefore, was controlled to less than 8.0 wt.%.

The basic morphologies of the composite membranes in the cross-sectional area were examined using a SEM. Since the composite membrane was prepared by overlaying three layers one by one, as expected, a three-layer structure for these composite membranes has been observed, as shown in Fig. 1(a). Closer SEM examination reveal that the top-layer and the bottom-layer are solid layers, and there exist some pores in the intermediate-layer. One of SEM images for the porous structure inside the inner layer is presented in Fig. 1(b).

Figs. 2 and 3 represent several typical plots of the complex impedance spectra for CH/G-B and CH/K-5 samples before and after hydration. In Fig. 2, both spectra comprise two distinct regions in the complex plane, a partial arc in the high frequency zone and a linear region in the low frequency zone, revealing the electrolyte characteristic of composite membranes in the dry state. However, the corresponding spectra of two composite membranes in their hydrated state have lost partial arc parts and their ionic resistance greatly decreases, indicating that

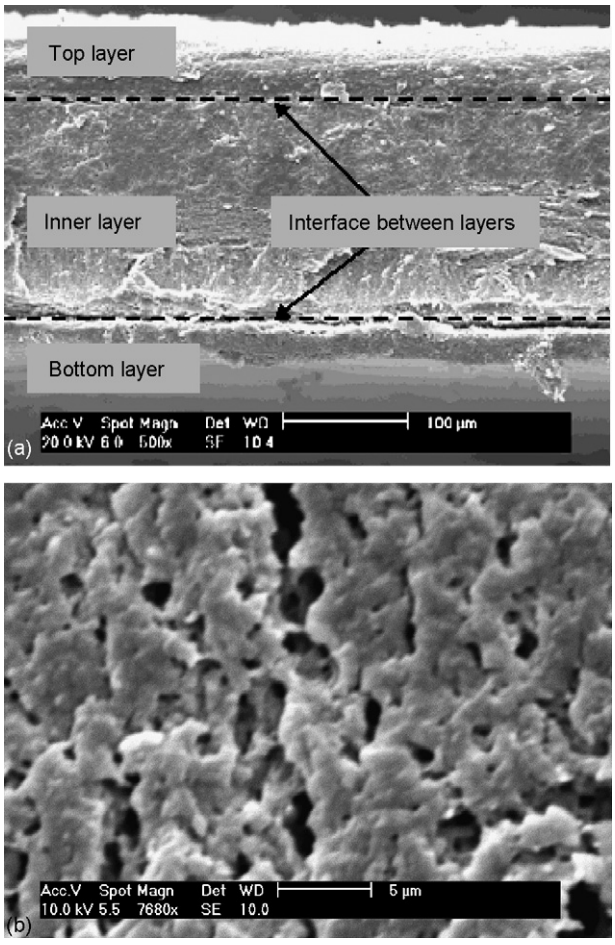

Fig. 1. SEM micrographs of the composite membranes. (a) Three-layer structure of composite membrane (CH/G-B); (b) porous structure of inner layer (CH/G-B).

the hydrated composite membranes, in fact, act basically like a common conductor. A few main parameters and calculated ionic conductivity from impedance spectra for two sets of samples are summarized in Table 1. Several characteristics can be drawn from Table 1: (1) it is not the GA/chitosan weight ratio

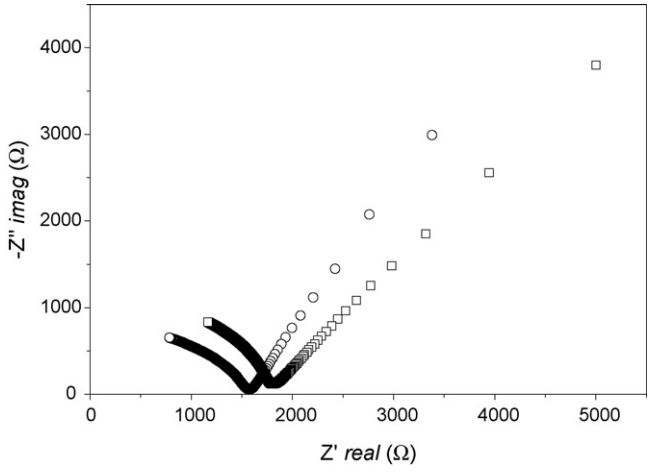

Fig. 2. Impedance spectra of the composite membranes in dry state. ◯, CH/G-B; □, CH/K-5.

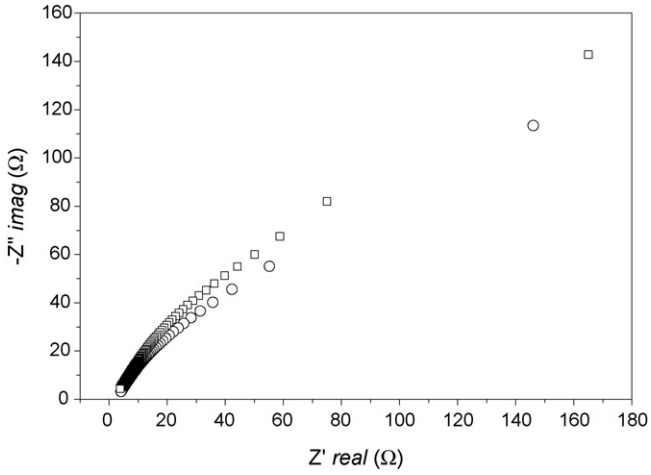

Fig. 3. Impedance spectra of the composite membranes after hydration for 1 h at room temperature. ◯, CH/G-B; □, CH/K-5.

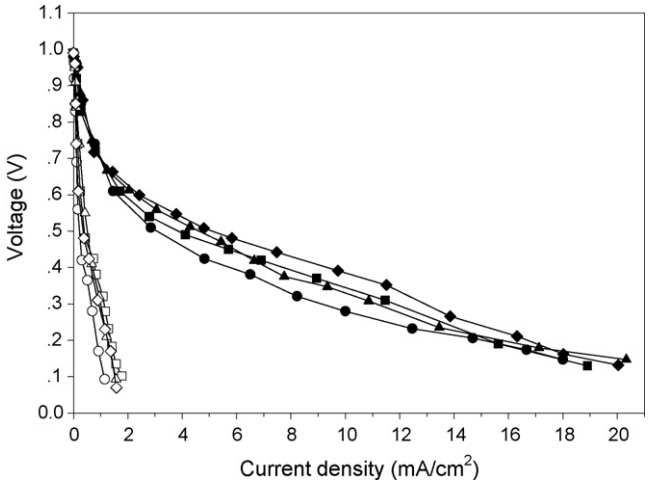

Fig. 4. Potential–current polarization curves of four cells using composite membranes in set of CH/K-*i* (*i* = 4–7) with relative humidity at 50% (unfilled symbols) and 100% (filled symbols). (Flow rate: 50 ml min^{-1} (H_2)/200 ml min^{-1} (air); temperature: 50 °C; pressure: $p(H_2) = p(air) = 103$ kPa). ◯, CH/K-4; ◇, CH/K-5; □, CH/K-6; △, CH/K-7; ●, CH/K-4; ■, CH/K-5; ♦, CH/K-6; ▲, CH/K-7.

but the concentration of KOH solutions that exerts an impact on the KOH content of the membranes; (2) dry composite membranes show a conductivity of around 10^{-6} S cm^{-1}, which is in the range for semi-conductors; (3) the hydrated composite membranes exhibit a higher conductivity near 10^{-2} S cm^{-1}, and their conductivity does not substantially vary with the GA/chitosan weight ratio, and only shows a slight change with the KOH content. Detailed analyses and explanations for these data can be found in another published report regarding the preparation and characterization as well as some properties of these composite membranes [38].

An ideal ionic conductivity of the hydrated polymer electrolyte membrane for the fuel cell operation is close to 10^{-2} S cm^{-1} or higher if only the conductivity is considered [39]. On the basis of the above observations, the GA/chitosan weight ratio does not substantially affect the conductivity of the hydrated membranes and all the hydrated composite membranes in the series CH/K-*i* (*i* = 4–7) possess a conductivity of around 10^{-2} S cm^{-1}, therefore, only those composite membranes in the CH/K-*i* (*i* = 4–7) set, which were prepared with a fixed GA/chitosan weight ratio (0.0555:1) but various concentrations of KOH solutions, were selected for further investigations in fuel cell testing.

3.2. Performance of fuel cells under basic running conditions

It is generally accepted that a relatively high cell pressure may help to improve the performance of a fuel cell. In our case, we encountered some difficulties such as the leakage of fuel and oxidant or a measurable fluctuation of the potential–current polarization curves if a high cell pressure was applied. The cell pressure ratio of hydrogen to air, hence, is selected as $p(H_2) = p(air) = 103$ kPa (at fixed flow rate of fuel, *p* is the initial of pressure) for the fuel cell measurements. In addition, it was also found that the effect of the relative humidity on the performance of the cell was quite pronounced. Fig. 4 illustrates several relevant potential–current polarization graphs. It is observed that with a relative humidity at 50%, the voltage of the cell sharply drops within a very narrow range related to the current density; on the other hand, a much better performance of the cells was achieved when the relative humidity reached 100%. As mentioned earlier, the chitosan membrane is highly hydrophilic due to its polar groups. A relative humidity at 100% certainly helps the chitosan membrane absorb water from the surrounding environment to the maximum limit and further to form more percolation pathways inside the membrane for ionic transport with the aid of gaps between ion aggregates in the membrane [40,41], and by doing this, the fuel cell would give a better performance [42]. Unfortunately, potential–current polarization curves relating to different relative humidities have not been systematically collected because the size of the unit cells is relatively small and the relative humidity between 50% and 100% cannot be exactly controlled. In the following testing, the relative humidity, therefore, was kept as constant at 100%.

3.3. Variation of performance of unit cell with composite membranes

Figs. 5 and 6 show several potential–current polarization curves based on a few different MEAs and measured in unit cells at 40 and 60 °C, respectively. These potential–current curves exhibit almost the same open-circuit potential of about 1.0 V both at 40 and at 60 °C. Meanwhile, it can be observed that (1) at the lower operation temperature, 40 °C, with respect to the same voltage, the current density of the cell using CH/K-7 or CH/K-6 membrane was comparably higher than that of the cell employing CH/K-4 membrane, but it was measurably lower than that of the cell utilizing a CH/K-5 membrane and (2) at an elevated operation temperature, 60 °C, an approximately similar performance was achieved when CH/K-7, CH/K-6 or CH/K-5 membranes were employed. These results indicate that the KOH content of composite membranes seems not to dominate the potential–current behavior of the cells and a

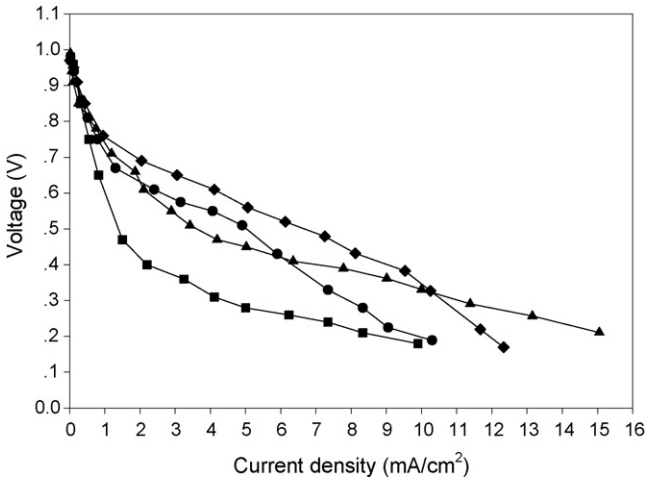

Fig. 5. Potential–current polarization curves of four cells. (Flow rate: 50 ml min^{-1} (H_2)/200 ml min^{-1} (air); temperature: 40 °C; pressure: $p(H_2) = p(air) =$ 103 kPa, relative humidity: 100%). ■, CH/K-4; ♦, CH/K-5; ▲, CH/K-6; ●, CH/K-7.

composite membrane with a higher conductivity is not likely to provide a cell with a better performance. Additionally, it is also noticed that the potential–current curves of cells can display measurable changes even if these cells use the same kind of MEAs which were fabricated using the composite membranes processed in the same batch with the exact same compositions (these variations are not presented here). A possible reason may arise from the interfacial properties of the membrane and electrodes because some defects in the surface of the membrane as well as nonuniformity in the thickness of the membrane could exert an influence on the properties of the MEA and in turn, the performance of the cell. Fig. 7 presents three SEM images CH/K-5 specimens (they were cut from the same kind of composite membranes prepared in the same batch under the exact same processing conditions, and coded as CH/K-5-a, CH/K-5-b, CH/K-5-c, respectively). It is apparent

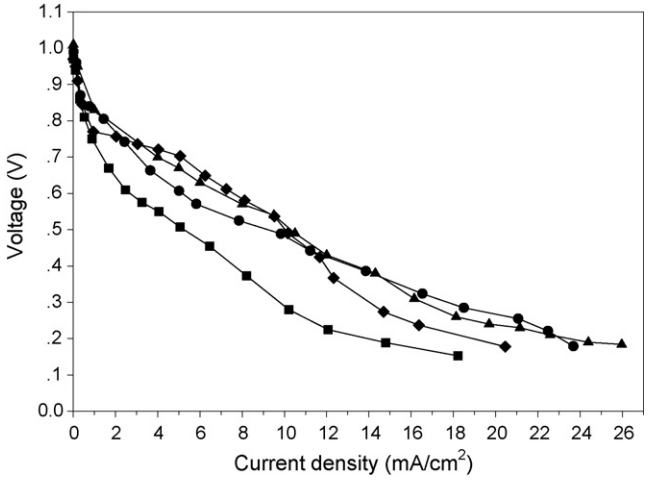

Fig. 6. Potential–current polarization curves of four cells. (Flow rate: 50 ml min^{-1} (H_2)/200 ml min^{-1} (air); temperature: 60 °C; pressure: $p(H_2) = p(air)$ = 103 kPa, relative humidity: 100%). ■, CH/K-4; ♦, CH/K-5; ▲, CH/K-6; ●, CH/K-7.

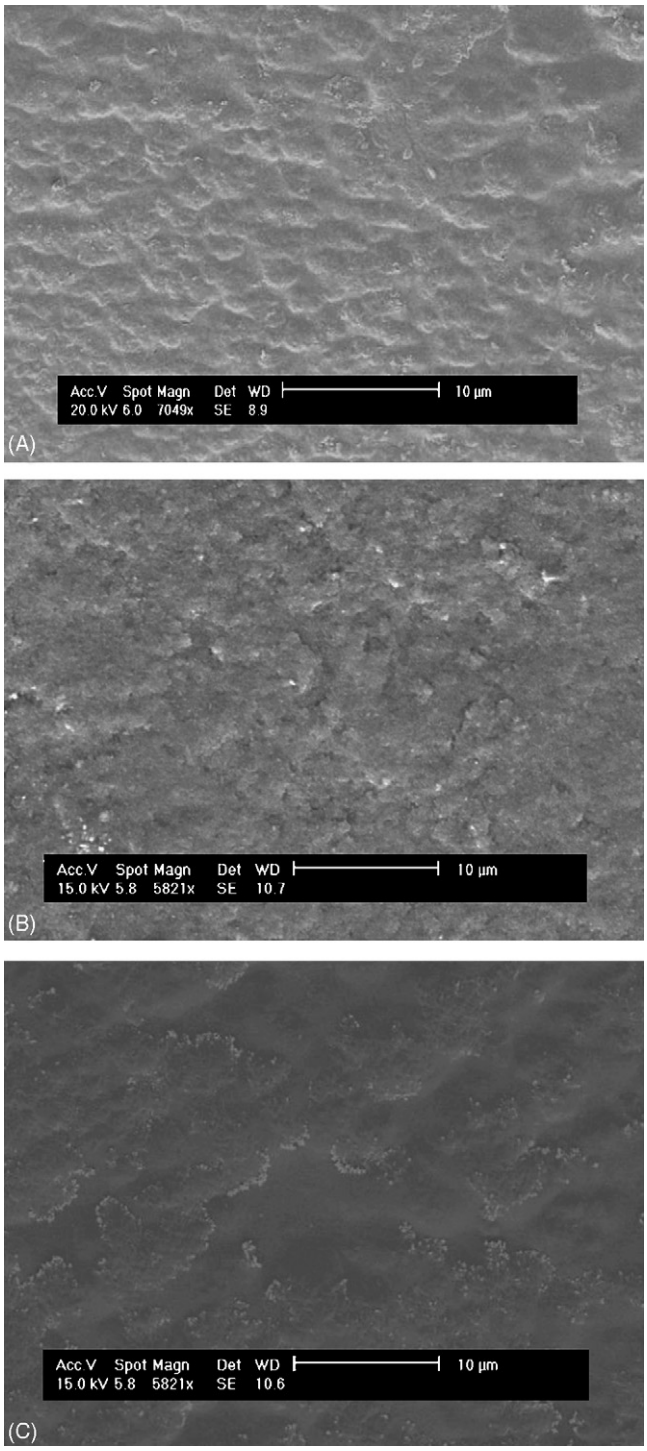

Fig. 7. Surface morphology of different specimens selected from CH/K-5 composite membranes in the same batch. (A) CH/K-5-a; (B) CH/K-5-b; (C) CH/K-5-c.

that the surface morphologies of the different specimens vary from one to another. Those easily viewed microscopic defects and nonuniformity will inevitably contribute to increasing the interfacial resistance between the membrane and the electrodes to some extent in a quite random way, and consequently the MEAs will also exhibit relatively irregular characteristics. The results illustrated in Figs. 5 and 6, therefore, should be related

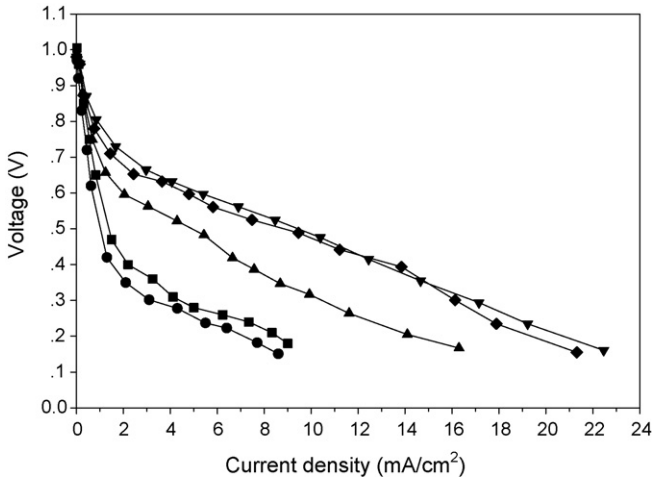

Fig. 8. Temperature dependence of potential–current polarization curves of cells (membrane: CH/K-4, flow rate: 50 ml min^{-1} (H_2)/200 ml min^{-1} (air); pressure: $p(H_2) = p(air) = 103$ kPa; relative humidity: 100%). ●, 40 °C; ■, 50 °C; ▲, 60 °C; ♦, 70 °C; ▼, 80 °C.

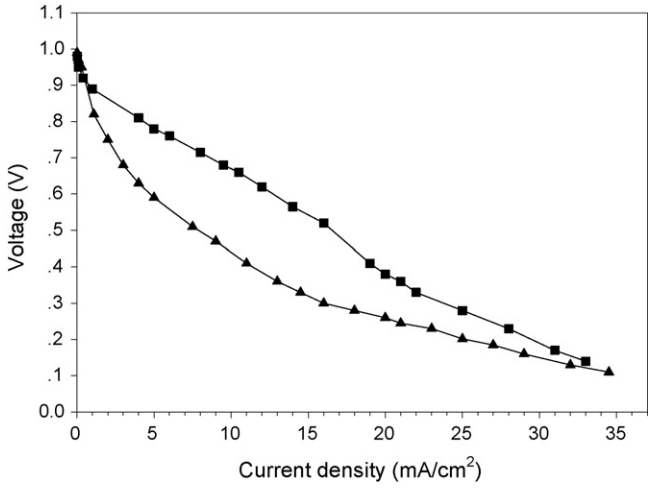

Fig. 9. Effect of flow rate of fuel on potential–current polarization curves (membrane: CH/K-6, temperature: 60 °C; pressure: $p(H_2) = p(air) = 103$ kPa, relative humidity: 100%). ▲, 50 ml min^{-1} (H_2)/200 ml min^{-1} (air); ■, 84 ml min^{-1} (H_2)/336 ml min^{-1} (air).

to a synergetic effect rising from the membrane's bulk conductivity and the interface properties between the membrane and electrodes.

3.4. Effect of temperature on the performance of cell

Since the KOH load inside the composite membrane has not significantly affected the performance of the cells, CH/K-4 was selected for investigating the temperature dependence of the cells, and the results are shown in Fig. 8. It can be seen that, with respect to the same voltage, the current density of the cell markedly increases as the operation temperature rises from 40 to 70 °C. However, a further increase in the operation temperature, for example, to 80 °C, does not substantially improve the performance of the cell. Possible reasons may lie in the following facts. In principle, a higher operation temperature not only promotes the catalytic reactions of electrodes but also facilitates the ions to migrate through the membrane [43], hence, a better performance could be achieved when a relatively high operation temperature is applied. Nevertheless, once a higher operation temperature is reached while the operation pressure is maintained as a constant, water will be more easily evaporated from one side of the membrane through which the hydroxide ions will migrate, which inevitably results in a decreased water content inside the composite membrane and, in turn, a lowered migration rate of hydroxide ions. As a consequence, the expected advantages possibly obtained from a higher operation temperature could be cancelled out by the decrease in the migration rate of hydroxide ions and the performance of the cell would not be improved further even at an elevated operation temperature. Based on the above observations, an appropriate running temperature should be controlled between 60 and 70 °C.

3.5. Effect of flow rate of fuel on the performance of cell

When the temperature, humidity and pressure of cell are selected as 60 °C, 100% and $p(H_2) = p(air) = 103$ kPa, respectively, and the flow rate of fuel is set at a ratio of 50 ml min^{-1} (H_2) to 200 ml min^{-1} (air) (the ratio of hydrogen to air is fixed at 1:4), it is observed that the cell can be continuously and stably run. With a further increase in flow rate to 84 ml min^{-1} (H_2)/336 ml min^{-1} (air), the cell performance was measurably improved. Fig. 9 shows two representative plots. It is seen that when the flow rate was increased from 50 ml min^{-1} (H_2)/200 ml min^{-1} (air) to 84 ml min^{-1}(H_2)/336 ml min^{-1} (air), the activation polarization (initial part of the curve) and the Ohmic polarization (middle part of the curve) of the plot matched with flow rate at 84 ml min^{-1}(H_2)/336 ml min^{-1} (air) are both stronger than with 50 ml min^{-1} (H_2)/200 ml min^{-1} (air). Meanwhile, when the current density reaches around 35 mA cm^{-2}, the potential of the cell dropped down to almost the same value: ca. 0.2 V for both plots. Potential–current curves at a flow rate higher than 84 ml min^{-1}(H_2)/336 ml min^{-1} (air) have not been given because they behave almost the same as the flow rate at 84 ml min^{-1}(H_2)/336 ml min^{-1} (air) in Fig. 9. These results may be explained based on following tentative mechanism. When the flow rate reached 50 ml min^{-1} (H_2)/200 ml min^{-1} (air), a just high enough concentration of oxygen and hydrogen inside both the cathode and anode was achieved for the electrodes to start continuous catalytic reaction and enable the cell to be stably operated. After that, since the total volume of voids inside the electrode is unchanged, an increase in the flow rate of air may first raise the concentration of oxygen at the cathode and then facilitate the catalytic reactions of both electrodes, leading to a stronger activation polarization of the cell by producing more OH groups at the cathode. As a result, a greater concentration gradient of OH groups over the membrane from the cathode to the anode would be established, which would further enhance the Ohmic polarization of the cell and provide the cell with a better performance. Once the flow rate was increased up to 84 ml min^{-1}(H_2)/336 ml min^{-1} (air), the concentration of oxygen and hydrogen may reach their respective saturation concentrations for the catalytic reactions

Table 2
Supplement parameters of the membrane and cell

Sample code	Average thickness (μm)[a]		IEC (meq g^{-1})	IR (mΩ)	OCP (V)
	Dry	Wet[b]			
CH/K-4	217 (±12)	389 (±31)	0.39 (±0.02)	46 (±5.3)	0.98 (±0.03)
CH/K-5	238 (±7)	367 (±26)	0.42 (±0.04)	42 (±3.6)	0.96 (±0.04)
CH/K-6	223 (±15)	379 (±34)	0.48 (±0.02)	49 (±8.2)	0.97 (±0.03)
CH/K-7	231 (±11)	392 (±29)	0.53 (±0.03)	44 (±7.1)	0.96 (±0.05)

[a] The average thickness is recorded as average values from five specimens for each sample.
[b] Hydration time for thickness measurements is 1 h.

of the electrodes and further increase in flow rate does not help the cell achieve improved performance.

3.6. Possible improvement on the performance of the resultant fuel cells

The above results reveal that current density of these alkaline fuel cells is still too low for practical application. A few other parameters may provide useful clues for improving the performance of the cells. Table 2 lists several supplemental parameters for the membrane in the CH/K-*i* (*i* = 4–7) set and the corresponding cells, including the average thickness of the dry membrane and the corresponding average thickness of the hydrated membrane, ion-exchange capacity (IEC) of membrane, internal resistance (IR) and open-circuit potential (OCP) of the cells.

In general, most practical polymer membrane fuel cells have an IR less than 3 mΩ and in some cases, the IR for an ideal value could be diminished to around 1 mΩ. The IR in Table 2 for four kinds of cells are all higher than 40 mΩ, which is over ten times higher than the IR value required and explains why the current density for those cells was low. The IR here should be mainly composed of two parts: the resistance of the composite membrane itself and the interfacial resistance between the membrane and electrodes. In Table 2, four kinds of dry membranes have an average thickness more than 200 μm, and after hydration for 1 h, the thickness of the membranes was increased to more than 350 μm. The membranes themselves, therefore, could contribute a considerable amount of resistance to the cell. In order to reduce the resistance of the membrane itself, one of effective approaches is to reduce the thickness of the membranes. Srinivasan et al. [44] evaluated the effect of membrane thickness on the performance of a cell, and reported that significant improvements on the performance of cell could be achieved using the thinner membranes. As for the decrease in the strength of the membrane due to the change in the thickness of membrane, it may be compensated by increasing the degree of crosslinking, which will also decrease the degree of swelling of the membrane and help to reduce the thickness of the corresponding hydrated membrane. Some efforts are being made to produce thinner composite membranes.

One of the most effective methods to fabricate MEAs is to press the electrodes onto the membrane at a proper temperature at which the two components can be very tightly bonded together, which will also possibly reduce the IR of the cell. However, in the present cases, by hot-pressing MEAs at various temperatures, we have not obtained any substantial improvement in the performance of the cells. The main reason may be ascribed to the too high glass transition temperature of chitosan, which is between 170 and 200 °C depending on the sources of chitosan and its DDA and molecular weight [45,46].

It has been reported that the interfacial resistance can be remarkably reduced by using appropriate interfacial gels with ionic-conductive characteristics [21,47–51]. The main mechanism is that the interfacial gels will fill in the voids between the membrane and electrodes, and thus the active surfaces and quantity of functional ions as well as the load of water molecules at the interface between the electrode and the membrane could be possibly increased, which would contribute to decreasing the interfacial resistance. An alkaline and high ionic-conductive gel is required for the present cells. However, several answers are still needed for an appropriate interfacial gel due to the specific properties of chitosan and so far investigations are still ongoing.

The IEC of the composite membrane listed in Table 2 is relatively low compared to the IEC of most commercial proton-exchange membranes [52–54]. Generally, the IEC is linked to the content of ions inside the membrane and the migration rate of the ions. Since the KOH load inside the membranes is high enough for ionic conductivity, it is expected that by reducing the thickness of the membranes and also regulating their degree of crosslinking, the IEC of the membranes could be further increased.

4. Conclusions

A preliminary evaluation on alkaline chitosan-based composite membrane fuel cells indicates that these membranes with a suitable KOH load are feasible for alkaline fuel cell applications although the power density of the resulting fuel cells are still low at present. At a lower running temperature, the performance of the fuel cell showed measurable changes with the KOH content but these changes became much less when the fuel cell was run at an elevated temperature. In addition, a relatively high running temperature provided the fuel cell with a much better performance. The current–potential characteristics were also significantly affected by the relative humidity. Additionally, the flow rate of the fuel can also affect the performance of these fuel cells. Under appropriate operation conditions, all obtained fuel cells showed an open-circuit potential of around 1.0 V. Under certain operation conditions, a current density of

about 30 mA cm^{-2} was achieved with a voltage of about 0.2 V. The performance of the fuel cell could be further improved by two approaches. One of them is to decrease the thickness of composite membranes and simultaneously enhance their physical strength, and the other approach is to use an alkaline and ionic-conductive interfacial gel.

Acknowledgements

This research was sponsored by the Natural Sciences and Engineering Research Council of Canada. The authors would like to acknowledge the assistances in fuel cell testing from Ms. Kathy Fulton.

References

[1] F.M. Gray, Solid Polymer Electrolytes, Fundamental and Technological Applications, VCH Publishers, New York, 1991.
[2] D.P. Wilkinson, Interface 10 (2001) 22.
[3] A.E. Steck, in: O. Savadogo, P.R. Roberge, T.N. Veziroglu (Eds.), Proceeding of the First International Symposium on New Materials for Fuel Cell Systems, Montreal, Canada, July 9–13, 1995, 1995, p. p.74.
[4] S. Hietala, M. Koel, E. Skou, M. Elomaa, F. Sundholm, J. Mater. Chem. 8 (1998) 1127.
[5] O. Savadogo, J. New Mater. Electrochem. Syst. 1 (1998) 47.
[6] M. Baldauf, W. Preidel, J. Power Sources 84 (1999) 161.
[7] A. Heinzel, V.M. Barragan, J. Power Sources 84 (1999) 70.
[8] S. Wasmus, A. Kuver, J. Electroanal. Chem. 416 (1999) 14.
[9] J.C. Amphlett, B.A. Peppley, E. Halliop, A. Sadiq, J. Power Sources 96 (2001) 204.
[10] O. Savadogo, Proceedings of the 13th World Hydrogen Energy Conference Vol. 2, Beijing, China, June12–15, 2000, p. p.756.
[11] G.F. McLean, T. Niet, S. Prince-Richard, N. Djilali, Int. J. Hydrogen Energy 27 (2002) 507.
[12] C. Lamy, E.M. Belgsir, J.M. Leger, J. Appl. Electrochem. 31 (2001) 799.
[13] E.H. Yu, K. Scott, R.W. Reeve, J. Electroanal. Chem. 547 (2003) 17.
[14] S. Gamburzev, K. Petrov, A.J. Appleby, J. Appl. Electrochem. 32 (2002) 805.
[15] K. Scott, P. Argyropoulos, P. Yiannopoulos, W.M. Taama, J. Appl. Electrochem. 31 (2001) 823.
[16] D.P. Davies, P.L. Adcock, M. Turpin, S.J. Rowen, J. Appl. Electrochem. 30 (2000) 101.
[17] A. Khalidi, B. Lafage, P. Taxil, G. Gave, M.J. Clifton, P. Cezac, Int. J. Hydrogen Energy 21 (1996) 25.
[18] M.T. Ergul, L. Turker, I. Erogul, Int. J. Hydrogen Energy 22 (1997) 1039.
[19] E. Guelzow, J. Power Sources 61 (1996) 99.
[20] X. Andrieu, J.F. Fauvarque, A. Goux, T. Hamaide, R. Mhamdi, T. Vicedo, Electrochim. Acta 40 (1995) 2295.
[21] E. Agel, J. Bouet, J.F. Fauvarque, J. Power Sources 101 (2001) 267.
[22] S. Guinot, E. Salmon, J.F. Penneau, J.F. Fauvarque, Electrochim. Acta 43 (1998) 1163.
[23] E. Salmon, S. Guinot, M. Godet, J.F. Fauvarque, J. Appl. Polym. Sci. 65 (1997) 601.
[24] B. Krajewska, J. Chem. Technol. Biotechnol. 76 (2001) 636.
[25] J.H. Kim, J.Y. Kim, Y.M. Lee, K.Y. Kim, J. Appl. Polym. Sci. 45 (1992) 1711.
[26] T.A. Zawodzinski, C. Derouin, S. Radzinski, R.J. Sherman, V.T. Smith, T.E. Springer, S. Gottesfeld, J. Electrochem. Soc. 140 (1993) 1041.
[27] Y.C. Wu, S.M. Hudson, J.M. Mayer, D.L. Kaplan, J. Polym. Sci. Part A: Polym. Chem. 30 (1992) 2187.
[28] Y. Wan, K.A.M. Creber, B. Peppley, V.T. Bui, J. Appl. Polym. Sci. 89 (2003) 306.
[29] Y. Wan, K.A.M. Creber, B. Peppley, V.T. Bui, E. Halliop, Polym. Int. 55 (2005) 5.
[30] R.A.A. Muzzarelli, C. Jeuniaux, G.W. Gooday, Chitin in Nature and Technology, Plenum, New York, 1986, pp. 385.
[31] S.C. Tan, E. Khor, T.K. Tan, S.M. Wong, Talanta 45 (1998) 713.
[32] Y. Wan, K.A.M. Creber, B. Peppley, V.T. Bui, Polymer 44 (2003) 1057.
[33] A. Mokrini, L.J. Acosta, Polymer 42 (2001) 8817.
[34] Z. Osman, Z.A. Ibrahim, A.K. Arof, Carbohydr. Polym. 44 (2001) 167.
[35] G.J. Hwang, H. Ohya, J. Membr. Sci. 140 (1998) 195.
[36] H. Herman, R.C.T. Slade, J.R. Varcoe, J. Membr. Sci. 218 (2003) 147.
[37] V.A. Davankov, M.P. Tsyurupa, Angew. Makromol. Chem. 91 (1980) 127.
[38] Y. Wan, K.A.M. Creber, B. Peppley, V.T. Bui, J. Membr. Sci. 280 (2006) 666.
[39] L.J.M.J. Blomen, M.N. Mugerwa, Fuell Cell System, Plenum, New York, 1993.
[40] H.L. Yeager, A. Steck, J. Electrochem. Soc. 128 (1981) 1880.
[41] K.A. Mauritz, C.E. Rogers, Macromolecules 18 (1985) 423.
[42] T.E. Springer, T.A. Zawodzinski, S. Gottesfeld, J. Electrochem. Soc. 138 (1991) 2334.
[43] J. Larminie, A. Dicks, Fuel Cell System Explained, 2nd ed., John Wiley and Sons, Chichester, England, 2003.
[44] S. Srinivasan, E.A. Ticianelli, C.R. Derouin, A. Redondo, J. Power Sources 22 (1988) 359.
[45] S.S. Kim, S.J. Kim, Y.D. Moon, Y.M. Lee, Polymer 35 (1994) 3212.
[46] M. Pizzoli, G. Ceccorulli, M. Scandola, Carbohydr. Res. 222 (1991) 205.
[47] M. Lefebvre, R.B. Martin, P.G. Pickup, Electrochem. Solid-State Lett. 2 (1998) 259.
[48] C. Gabrielli, O. Hass, H. Takenouti, J. Appl. Electrochem. 17 (1987) 82.
[49] S.S. Kocha, in: W. Vielstich, A. Lamm, H.A. Gasteiger (Eds.), Handbook of Fuel Cell, Volume 3, Fuel Cell Technology and Applications, Part 1, John Wiley & Sons, Milan, Italy, 2003, pp. 538–565.
[50] W.G. Grot, US Patent, 5,547,911 (1996).
[51] J.S. Hulett, US Patent 6,074,692 (2000).
[52] P. Brack, H.H.G. Bushrer, L. Bonorand, G.G. Scherer, J. Mater. Chem. 10 (2001) 1795.
[53] K.V. Lovell, J.A. Horsfall, Eur. Polym. J. 38 (2002) 1671.
[54] Z. Ogumi, K. Matsuoka, S. Chiba, M. Mastuoka, Y. Iriyama, T. Abe, M. Inaba, Electrochemistry 70 (2002) 980.